Propagation of extremely high energy leptons in Earth: Implications for their detection by the IceCube neutrino telescope

Shigeru Yoshida,* Rie Ishibashi,† and Hiroko Miyamoto
Department of Physics, Faculty of Science, Chiba University, Chiba 263-8522, Japan
(Received 12 December 2003; published 17 May 2004)

We present the results of numerical calculations on the propagation of extremely high energy (EHE) neutrinos and charged leptons in Earth for trajectories in the whole phase space of nadir angles. Our comprehensive calculation has shown that not only the secondary produced muons but also taus survive without decaying in the energy range of 10–100 PeV with an intensity approximately three orders of magnitude lower than the neutrino flux regardless of the EHE neutrino production model. They form detectable horizontal or downgoing events in a 1 km^3 underground neutrino telescope such as the IceCube detector. The event rate and the resulting detectability of EHE signals in comparison with the atmospheric muon background are also evaluated. The 90% C.L. upper limit of EHE neutrino fluxes by a km^2 detection area would be placed at $E^2dF/dE \simeq 3.7 \times 10^{-8}$ GeV/cm^2 sec sr for ν_μ and 4.6×10^{-8} for ν_τ with energies of 10^9 GeV in the absence of signals with an energy loss in a detection volume of 10 PeV or greater.

DOI: 10.1103/PhysRevD.69.103004 PACS number(s): 98.70.Sa, 95.85.Ry, 98.70.Vc, 98.80.Cq

I. INTRODUCTION

It is well known that there exist extremely high energy (EHE) particles in the Universe with energies up to $\sim 10^{20}$ eV [1]. These EHE cosmic rays (EHECRs) may originate in and/or produce neutrinos by various mechanisms. For example, collisions of EHECRs and cosmic microwave background (CMB) photons photoproduce cosmogenic neutrinos [2], a consequence of the process known as the Greisen-Zatsepin-Kuzmin (GZK) mechanism [3]. The possible production of EHECRs in the present Universe due to the annihilation or collapse of topological defects (TDs) such as monopoles and/or cosmic strings [4] could also generate EHE neutrinos with energies even reaching grand unified theory (GUT) scale [5,6]. EHE neutrinos provide, therefore, a unique probe to explore the ultrahigh energy Universe, which is one of the centerpieces of high energy neutrino astrophysics.

It has been argued that the underground neutrino telescopes being operated and/or planned to be built are capable of detecting such EHE neutrinos [7]. In their travel through Earth to the detection volume in a telescope, EHE neutrinos collide with nuclei in rock due to the enhancement of the cross section at EHE range and produce secondary leptons such as muons and taus. The expected mean free path is $\sim 600(\rho_{rock}/2.65\ \mathrm{g\,cm^{-3}})^{-1}(\sigma_\nu/10^{-32}\ \mathrm{cm^2})^{-1}$ km which is far shorter than the typical path length of the propagation in Earth. Moreover, the decay lifetime is long enough at EHEs for the produced μ and τ to survive and possibly reach the detection volume directly. Successive reactions of interaction and decay are likely to occur in their propagation, and the propagation processes of EHE particles are rather complex. The accurate understanding of the EHE neutrino and charged lepton propagation in the earth is, thus, inevitable for an EHE neutrino search by underground neutrino telescopes.

There has been considerable discussion in the literature from this point of view. In Ref. [8], the transport equations mainly focusing on ν_τ and τ were solved and the resulting particle fluxes after propagation have been shown for trajectories of several nadir angles in the horizontal directions such as 85°. It is true that a major fraction of EHE τ tracks are coming from the horizontal directions because Earth is opaque for EHE neutrinos, but a km^3 scale neutrino observatory such as IceCube is essentially a 4π detector with comparable sensitivities to both muons and taus, and calculation of the EHE particle energy spectra of both muons and taus over the whole solid angle space including downward event trajectories would be important to evaluate detectability with reasonable accuracy. Furthermore, they utilized the often used continuous energy loss (CEL) approximation that follows only the leading cascade particles. It is a good approximation for taus, but the secondary particle fluxes contributed from the nonleading particles are not negligible for muons at EHEs where their decay does not play a visible role. Calculations on the Earth-skimming EHE ν_τ have also been made in some detail [9]. These authors used approximations to neglect the contributions of the leptons generated from tau interactions and decay in Earth, which would be valid enough for consideration of Earth-skimming neutrino-induced air showers. It has been pointed out, however, that the secondarily produced ν_e and ν_μ from tau decay would also enhance the total neutrino flux [10], which would be a benefit for an underground neutrino observatory. Following all propagating leptons and taking into account the contributions from particles not only skimming but propagating deeper in Earth are, therefore, essential for an underground-based neutrino observatory.

In this work, we numerically calculate the intensity and energy distribution of EHE neutrinos and their secondarily produced μ's and τ's during propagation in Earth for the

*Electronic address: syoshida@hepburn.s.chiba-u.ac.jp; URL: http://www.ppl.phys.chiba-u.jp/

†Now at Ushio Denki, Co.Ltd., 2-6-1 Oote-machi, Chiyoda-ku, Tokyo 100-0004, Japan.

application to a km^3 scale neutrino observatory. The resulting fluxes are shown as a function of nadir angle from downward to upward going directions. All the relevant interactions are taken into account and we follow *all* particles produced in the reactions whereas the CEL approximation follows only the leading cascade particles. The initial flux is mainly assumed to be the bulk of the cosmogenic neutrinos, generated from the decay of pions photoproduced by EHE cosmic ray protons colliding with the cosmic thermal background photons, since the cosmogenic neutrino model is appropriate as a benchmark as the flux prediction is on the solid theoretical foundation. Its implications for detection by the IceCube neutrino telescope [11], which is currently under construction at Antarctica, are then discussed in some detail.

The paper is outlined as follows. First we briefly review the interaction and decay channels involved with EHE particle propagation in Earth in Sec. II. The method of our numerical calculations is also briefly explained. In Sec. III we show the calculated results: the energy distributions and intensities of muons, taus, and neutrinos after their propagation. The energy spectra of these EHE particles are shown for the cosmogenic neutrino model. Implications on the detection by the IceCube neutrino telescope are discussed in Sec. IV and the detectability considering the possible background in the experiment is discussed in detail. The sensitivity to EHE neutrino fluxes by a km^3 neutrino observatory is also shown. We summarize our conclusions and make suggestions for future work in Sec. V.

II. DYNAMICS OF THE PROPAGATION IN EARTH

EHE neutrinos during propagation do not penetrate Earth but are involved in charged or neutral current interactions that generate charged leptons and hadronic showers because their cross sections are expected to be enhanced in the ultrahigh energy regime. Secondarily produced μ's and τ's travel in Earth, initiating many radiative reactions to lose their energy. Higher order interactions like $\mu^{\pm}$ pair production [12] and charged current disappearance reactions like $\mu N \to \nu_\mu X$ regenerate charged leptons and neutrinos which are subject to further interactions. Moreover, the τ's decay channels like $\tau \to \nu_\tau \mu \nu_\mu$ regenerate ν_τ. A primary EHE neutrino particle, therefore, results in a number of particles with various energies and species which would pass through an instrumented volume of an underground neutrino telescope. The resulting energy spectra and their intensities are consequences of the chain processes of interaction and decay. Table I summarizes the interaction and decay channels as a function of primary and generated particle species. The main energy loss process for secondarily produced μ's and τ's are $e^{\pm}$ pair creation, bremsstrahlung, and photonuclear interactions. The relevant cross sections are formulated in Ref. [13] for pair creation, Ref. [14] for bremsstrahlung, and Ref. [15] for photonuclear interaction. Among these the photonuclear cross section has the largest theoretical uncertainty because it relies on the details of the nuclei structure function, which has to be estimated from extrapolation from the low energy data. In the present calculation we use the estimation based on the deep-inelastic scattering formalism with the Abramowicz-Levin-Levy-Maor (ALLM) parameterization of the structure function [16], which is considered to be the most reliable prediction. We artificially switch off the photonuclear interaction to see its systematic uncertainty in the results later in this paper. Furthermore, the weak interaction $l^{\pm}N \to \nu X$ causing muon and tau disappearances, and the heavier lepton pair production such as $\mu^+\mu^-$ [12], are also taken into account in the present calculation, which leads to a visible contribution to the particle fluxes at EHEs.

TABLE I. Interactions and decay channels involved in the EHE particle propagation in Earth. Rows are primary and columns are generated particles.

	ν_e	ν_μ	ν_τ	e/γ	μ	τ	hadron
ν_e	NC [a]			CC [b]			CC/NC
ν_μ		NC			CC		CC/NC
ν_τ			NC			CC	CC/NC
μ	D [c]	D/CC		P [d]/B [e]/D	P	P	PN [f]/CC
τ	D	D	D/CC	P/B/D	P/D	P	PN/CC/D

[a]Neutral current interaction.
[b]Charged current interaction.
[c]Decay.
[d]Pair creation.
[e]Bremsstrahlung.
[f]Photonuclear interaction.

An EHE neutrino is subject to charged current (CC) and neutral current (NC) interactions with nucleons. As there is no direct measurement of the relevant interactions in the EHE range, the predictions for the νN cross sections rely on incompletely tested assumptions about the behavior of parton distributions at very small values of the momentum fraction x. Since we do not have further clues to investigate EHE neutrino interactions in our hands, we limit our present analysis to the range of standard particle physics and use the cross section estimated by Ref. [17] using the CTEQ version 5 parton distribution functions [18].

Decay processes are also major channels and compete with the interaction processes depending on energy. The μ and τ leptonic decay distribution can be analytically calculated from the decay matrix using the approximation that the generated lepton mass is negligible compared to that of the parent lepton [19]. For $z = E_{\nu_l}/E_l$ ($l = \mu$ or τ) it is written as

$$\frac{dn}{dz} = \frac{5}{3} - 3z^2 + \frac{4}{3}z^3 - \left(\frac{1}{3} - 3z^2 + \frac{8}{3}z^3\right), \tag{1}$$

and for $y_\nu = E_{\nu_e}/E_\mu$ (μ decay), $E_{\nu_{e,\mu}}/E_\tau$ (τ decay),

$$\frac{dn}{dz} = 2 - 6y_\nu^2 + 4y_\nu^3 - (-2 + 12y_\nu - 18y_\nu^2 + 8y_\nu^3). \tag{2}$$

The hadronic τ decay has various modes and its accurate treatment is rather difficult. Here we use the two-body decay approximation as in Ref. [20].

The transport equations to describe particle propagation in Earth are given by

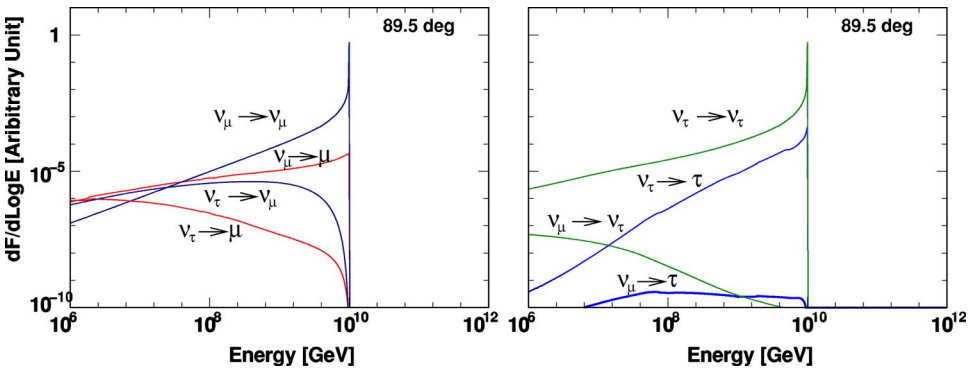

FIG. 1. The energy distribution of EHE leptons after propagation in Earth with nadir angle of 89.5°. μ's and τ's are secondarily produced. The left panel shows the distributions of leptons with μ flavor while the right panel shows the case of τ flavor. The input spectrum is 10^{10} GeV monochromatic with ν_μ and ν_τ having equal intensity of 1 in these arbitrary units.

$$\frac{dJ_\nu}{dX} = -N_A \sigma_{\nu N,CC+NC} J_\nu + \frac{m_l}{c\rho\tau_l^d} \int dE_l \frac{1}{E_l} \frac{dn_l^d}{dE_\nu} J_l(E_l) + N_A \int dE'_\nu \frac{d\sigma_{\nu N,NC}}{dE_\nu} J_\nu(E'_\nu) + N_A \int dE'_l \frac{d\sigma_{lN,CC}}{dE_\nu} J_l(E'_l), \tag{3}$$

$$\frac{dJ_l}{dX} = -N_A \sigma_{lN} J_l - \frac{m_l}{c\rho\tau_l^d E_l} J_l + N_A \int dE'_\nu \frac{d\sigma_{\nu N,CC}}{dE_l} J_\nu(E'_\nu) + N_A \int dE'_l \frac{d\sigma_{lN}}{dE_l} J_l(E'_l) + \frac{m_l}{c\rho\tau_l^d} \int dE'_l \frac{1}{E'_l} \frac{dn_l^d}{dE_l} J_l(E'_l), \tag{4}$$

where $J_l = dN_l/dE_l$ and $J_\nu = dN_\nu/dE_\nu$ are the differential fluxes of charged leptons and neutrinos, respectively, N_A is Avogadro's number, ρ is the local density of the medium (rock/ice) in the propagation path, σ is the relevant interaction cross section, dn_l^d/dE is the energy distribution of the decay products, which is derived from the decay rate per unit energy and given by Eqs. (1) and (2), c is the speed of light, and m_l and τ_l^d are the mass and the decay lifetime of the lepton l, respectively. The density profile of the rock, $\rho(L)$, is given by the preliminary Earth model [21]. A column density X is defined by $X = \int_0^L \rho(L')dL'$.

Equation (3) describes neutrino propagation. The first term is a loss due to the neutrino interaction, the second represents a contribution due to the decay, and the rest of the terms account for generation of neutrinos by the neutrino and charged lepton interactions. The fourth term represents neutrino appearance by CC interactions such as $\mu N \to \nu_\mu X$. Equation (4) describes charged lepton propagation and has similar terms to those of Eq. (3), but also a term to represent loss due to lepton decay.

We calculated these equations numerically by building the matrices describing the particle propagation over infinitesimal distances as described in Refs. [22,23]. The energy differential cross sections are derived from the ones for the inelasticity parameter $y = 1 - E'/E$, i.e., $d\sigma/dy$. Let us show two examples to show the behavior of the EHE particle propagation in Earth. Figure 1 shows the energy distribution of EHE leptons after propagation in Earth, entering with nadir angle of 89.5°. The corresponding propagation distance in Earth is ~110 km. The primary input spectrum is a monochromatic energy distribution of 10^{10} GeV of ν_μ and ν_τ with equal intensities. Sizable amounts of the secondarily produced μ's and τ's are found. As the μ bulk from ν_τ is mainly generated from τ decay, which occurs less frequently in the high energy region, their intensity decreases with higher energy. For the same reason, the secondary τ energy distribution is harder than that of μ's. Note that τ originated in primary ν_μ denoted as $\nu_\mu \to \tau$ in the right panel in the figure are produced in heavy lepton pair creation $\mu \to \mu\tau^+\tau^-$.

The intensities of "prompt" muons and taus, whose energies are approximately the same as those of the primary neutrinos, are four to five orders of magnitude lower than the primary neutrino flux as indicated in the figures, but the low energy bulk of the secondary muons and taus which have suffered energy loss during their propagation makes a significant contribution to the flux for a given neutrino energy spectrum. It should also be remarked that the muons generated from secondarily produced tau decay, denoted as $\nu_\tau \to \mu$, constitute a major fraction of the intensity below 10^8 GeV. We see in the next section that they form a sizable flux for the EHE neutrino model producing a hard energy spectrum like the cosmogenic neutrinos generated by the GZK mechanism.

When particles are propagating more vertically upward, i.e., their propagation distance is longer, all the prompt component disappears and no particles essentially survive in the EHE range, because of the significant energy losses. A typical case is shown in Fig. 2 for nadir angle of 70°. One can see that most of the secondary muons and neutrinos are absorbed and they remain only in the low energy range.

The energy distributions and intensities of EHE particles propagating in Earth are, consequently, strongly dependent on the zenith (or nadir) angle of the trajectory, and also on the initial neutrino energy spectrum. One must solve the transport equation in the entire phase space in the zenith angle in order to make accurate estimations of the fluxes we see in an underground neutrino telescope for a given neutrino initial flux.

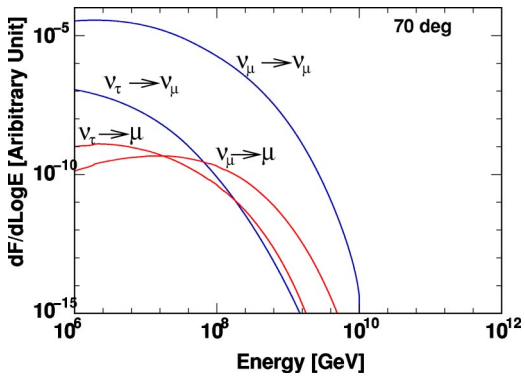

FIG. 2. Same as Fig. 1, but for nadir angle of 70°. Shown are the distributions of leptons with μ flavor when the input ν_μ and ν_τ is monochromatic energy of 10^{10} GeV.

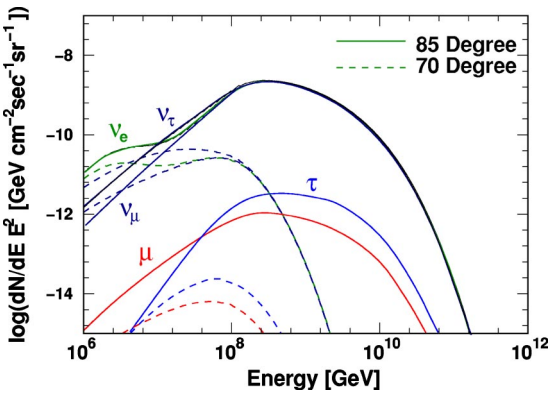

FIG. 3. Fluxes of EHE particles at the IceCube depth for the scenario of neutrino production by the GZK mechanism. Two cases of nadir angle are shown in the figure.

III. THE COSMOGENIC NEUTRINO FLUX AT UNDERGROUND DEPTH

In this section, we discuss the case when the initial fluxes of ν_μ and ν_τ are given by the GZK mechanism, EHE neutrino production by collisions of EHECRs with CMB photons in extragalactic space, as this model has been thought to be the most conventional mechanism to generate EHE neutrinos without new physics and/or speculative assumptions. The biggest uncertainty in the intensity of the cosmogenic fluxes is related to the cosmic ray source distributions. Assuming homogeneously distributed astrophysical sources, however, variations of the magnitude of the neutrino flux above 10^9 GeV are restricted approximately within a factor of 10 [24]. Although assuming an extremely hard cosmic ray injection spectrum like $\sim E^{-1}$ or very strong source evolution allows larger fluxes which can still be consistent with the EHECRs and the EGRET γ-ray observations [25], here we limit the present calculations to the conventional case that homogeneously distributed astrophysical sources are responsible for the observed EHECR flux below 10^{20} eV.

We solve Eqs. (3) and (4) to evaluate the particle fluxes at an underground depth where a kilometer-scale neutrino observatory is expected to be located. The IceCube neutrino telescope is constructed at 1400 m depth below the ice surface and we take this number as a representative depth. It has been found that changing this depth within a factor of 2 would not affect the overall EHE particle intensity in a significant manner and the conclusion remains the same. Neutrino oscillation with full mixing is assumed and the ν_μ initial flux is identical to that of ν_τ. For the parameters constrained by the SuperK experiment [26], the oscillation probability in the earth in the EHE range is negligible, however, and we do not account for the oscillation in the present calculation on propagation.

Figure 3 shows the fluxes with nadir angle of 85° and 70°. The initial primary cosmogenic neutrino fluxes are taken from Ref. [22]. Taus notably dominate muons because their heavy mass makes them penetrate Earth and because decay is less important than interactions for the relevant energy range. The case of nadir angle of 70° exhibits the strong attenuation, however, due to the fact that the mean free paths of all the relevant interactions including the weak interactions of neutrinos are far shorter than the propagation distance. This implies that most of the upgoing events in a neutrino observatory come from horizontal directions.

The ν_τ flux becomes dominating over that of ν_μ in the low energy range where the τ decay is significantly more important than interactions. This enhancement is caused by the $\nu_\tau \rightarrow \tau \rightarrow \nu_\tau$ regeneration process. Note that the small bump in the ν_e spectrum is not a propagation effect but generated primarily by EHECR neutron decay in space [22,24].

The intensity strongly depends on the nadir angle. Figure 4 shows the dependence of the secondary muon and tau fluxes on the zenith angles. Strong attenuation by Earth can be seen but the fluxes are more or less stable in the region of the "downward" events where $\cos\theta \geqslant 0$. Particles in this range are propagating in ice ($\rho = 0.917$ g/cm^3) to enter into the detection volume. We numerically solved the transport equation in the ice medium to derive the downward fluxes. The downward fluxes constitute a major fraction of events in an underground neutrino observatory. The detection issues are discussed in Sec. IV.

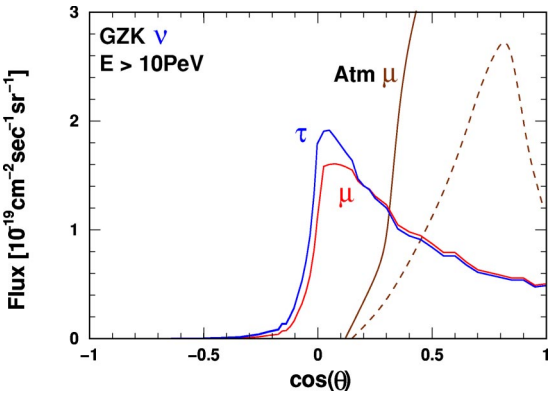

FIG. 4. Dependence of the muon and tau fluxes originating in the cosmogenic neutrinos on the cosine of zenith angle. The integrated flux above 10 PeV is plotted on a linear scale. The atmospheric muon fluxes are also shown by the solid curve for a conservative estimation with low energy extrapolation and by the dashed curve for a CORSIKA-based estimation. The details of the atmospheric fluxes are discussed in Sec. IV.

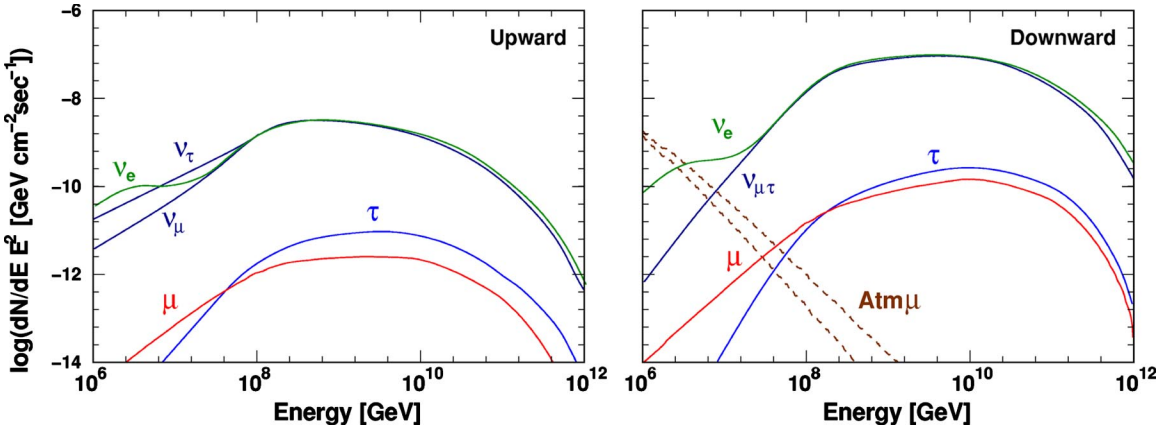

FIG. 5. Energy spectra of $\nu_e, \nu_\mu, \nu_\tau, \mu, \tau$ originating in the cosmogenic neutrinos at the IceCube depth. The intensities are integrated over solid angle and shown for the upward region ($\cos\theta \leqslant 0$, left panel) and the downward region ($\cos\theta \geqslant 0$, right panel). The two dashed lines represent the atmospheric muon intensities. The upper line shows a conservative estimation based on simple extrapolation from the calculation at 5 TeV, while the lower line is derived by Monte Carlo simulation with the CORSIKA package.

The energy spectra integrated over zenith angle are shown in Fig. 5. Secondary muons and taus form a potentially detectable bulk with intensity $\sim$ three orders of magnitude lower than the neutrino fluxes. The main energy range is 10 PeV to 10 EeV ($=10^{10}$ GeV). Regardless of the neutrino production model, the intensity of μ and τ relative to ν_μ and ν_τ remains approximately unchanged. It should be remarked that the intensity of the downward going muons and taus is larger than the upward one by an order of magnitude. As also seen in Fig. 3, the tau flux dominates over the muons above 10^8 GeV. Enhancement of ν_τ intensity by regeneration also appears in the upward going trajectories.

The uncertainty in the muon and tau flux estimations mainly arises from the fact that we do not know the photonuclear cross section accurately in the EHE range. For example, using the updated approach to deduce the photonuclear cross section including the soft part of the photonuclear interaction would lead to $\sim$30% enhancement of the total tau energy loss in the EHE range [27]. To be conservative, in Fig. 6 we show a comparison of the fluxes with and without photonuclear reactions. Switching off the photonuclear interactions results in a factor of 2 variance in the intensity, which would represent the error range of the secondary tau flux estimations in a conservative manner.

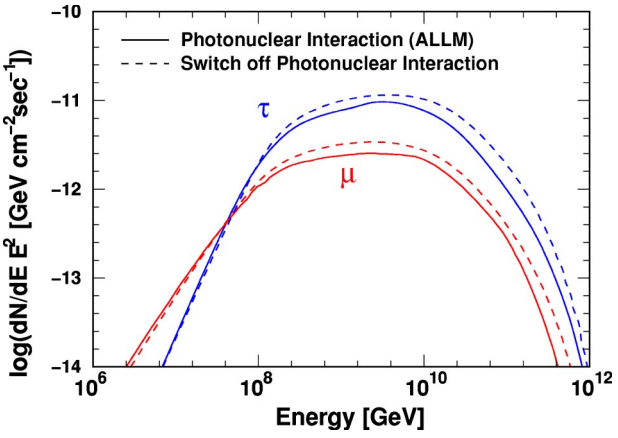

FIG. 6. Dependence of the muon and tau upward fluxes on photonuclear interactions. The integrated fluxes over nadir angles of 0° to 90° are shown.

IV. DETECTION BY A KILOMETER-SCALE NEUTRINO OBSERVATORY

The event rate for a neutrino observatory can be estimated by integrating the energy spectra shown in Fig. 5 above a threshold energy multiplied by the effective area of the detector, which is 1 km^2 in the case of IceCube. The downward events are major contributions and it is necessary to consider the atmospheric muon background, however. The atmospheric muon flux estimation in the relevant energy range is not straightforward because there is no measurement available and numerical calculation is also time consuming as one must fully simulate EHE air shower cascades. Here we use two methods to estimate the flux. One is to extrapolate the calculation at 5 TeV [28] which has been confirmed to be consistent with the measurement. Because the cosmic ray energy spectrum follows $E^{-2.7}$ in the TeV region while high energy cosmic ray spectra above 10 PeV are steeper, following E^{-3}, this extrapolation would overestimate the flux, but it gives a conservative evaluation. The other method is to run the CORSIKA air shower simulation [29] with the energy spectrum of the observed E^{-3} dependence under the assumption that the whole mass composition is protons, and count the number of high energy muons reaching the ground. Then we solve the transport equations for the derived muon fluxes at the surface. The results obtained for the background intensity in downward events are shown in the right panel of Fig. 5 by two dashed lines. One can see that the muon background spectrum is quite steep. Setting a higher threshold energy, therefore, would allow elimination of the background contamination. The flux dependence on the zenith angle is shown in Fig. 4 when the threshold energy is 10 PeV. It is clearly seen that the muon background attenuates faster than the neutrino-induced EHE muons and taus, and there is a window where the signals dominate the muon background. Table II summarizes the intensity with threshold energy of 10

TABLE II. Integral flux intensities for several EHE neutrino models.

	$I_{\nu_{\mu,\tau}}(E \geqslant 10\ \mathrm{PeV})$ [a] $(\mathrm{cm}^{-2}\,\mathrm{sec}^{-1}\,2\pi^{-1})$	$I_{\mu}(E \geqslant 10\ \mathrm{PeV})$ $(\mathrm{cm}^{-2}\,\mathrm{sec}^{-1})$	$I_{\tau}(E \geqslant 10\ \mathrm{PeV})$ $(\mathrm{cm}^{-2}\,\mathrm{sec}^{-1})$	$I_{\mu}(E_{loss} \geqslant 10\ \mathrm{PeV})$ $(\mathrm{cm}^{-2}\,\mathrm{sec}^{-1})$	$I_{\tau}(E_{loss} \geqslant 10\ \mathrm{PeV})$ $(\mathrm{cm}^{-2}\,\mathrm{sec}^{-1})$
GZK [b] downward	5.97×10^{-16}	5.90×10^{-19}	5.97×10^{-19}	4.75×10^{-19}	3.28×10^{-19}
GZK upward	5.97×10^{-16}	3.91×10^{-20}	6.63×10^{-20}	2.57×10^{-20}	2.64×10^{-20}
TD [c] downward	9.92×10^{-15}	5.48×10^{-18}	5.11×10^{-18}	3.75×10^{-18}	2.94×10^{-18}
Atmospheric μ	—	2.06×10^{-18}	—	1.74×10^{-19}	—
Atmospheric μ [d]	—	7.25×10^{-19}	—	5.34×10^{-20}	—

[a]Intensity at surface before propagating in Earth.
[b]Cosmogenic neutrinos with $(m, Z_{max}) = (4.0, 4.0)$ in Ref. [22].
[c]Topological defect scenario using supersymmetry-based fragmentation function in Ref. [6].
[d]Estimation based on the CORSIKA simulation.

PeV for the various EHE neutrino models together with those of the atmospheric muon background.

In fact, what neutrino detectors can measure in a direct manner is not the energy of muon or tau tracks but the energy loss in the detection volume. The relation between energy and energy loss is approximately $-dE/dX \sim \beta E$. Here β is the average inelasticity given by

$$\beta = \int_{y_{min}}^{y_{max}} dy' y' \frac{d\sigma}{dy'}. \tag{5}$$

For the $e^{\pm}$ pair creation of muons in ice, $\beta \simeq 1.3 \times 10^{-6}$ cm^2/g. Therefore the average energy loss fraction due to the pair creation is

$$\frac{\Delta E}{E} \simeq \beta^{e^{\pm}} \Delta X$$

$$= 0.12 \left(\frac{\beta^{e^{\pm}}}{1.3\times10^{-6}} \right) \left(\frac{\rho_{ice}}{0.92\ \ \mathrm{g\,cm}^{-2}} \right) \left(\frac{\Delta L}{1\ \ \mathrm{km}} \right), \tag{6}$$

indicating that 10% of the muon primary energy is deposited in a detection volume. Because radiative interactions like bremsstrahlung have a stochastic nature, ΔE fluctuates significantly on an event by event basis, however. We carried out a Monte Carlo simulation to see the fluctuation. The simulation code uses the same cross section and decay tables but calculates the energy of a particle after an infinitesimal propagation length ΔX with the Monte Carlo method instead of solving the transport equations. Figure 7 shows the distribution of the energy loss of muons in running over 1 km in ice. The energy loss distribution due to the pair creation may be narrow enough for the CEL approximation; this is not the case for the distributions due to the other interactions, however. It is not appropriate to approximate the entire distribution by a δ function, which implies that the energy *loss* rather than the energy would be better to describe the event characteristics.

As a more realistic criterion, we introduce the threshold of the energy loss in ice instead of the energy itself. Figure 8 shows the GZK integrated flux dependences on the zenith angle in the case of the 10 PeV threshold of the energy loss. One can see in comparison to Fig. 4 that the GZK fluxes are larger than or comparable to the muon background intensity in all the zenith directions in this energy-loss-based criterion. This indicates that it is probable that an EHE neutrino search using downward events can be made under an almost background-free environment.

It should be noted that the tau flux is lower than the muon flux with this criterion. This is because the heavier mass of the tau suppresses the energy loss compared to that of muons with the same energy. This situation is illustrated in Fig. 9 where the tau fluxes are plotted as functions of energy and energy loss in ice during 1 km propagation. The intensity above 10^7 GeV is reduced because of the energy loss suppression. Higher energy loss takes place in the form of hadronic cascades initiated by the photonuclear interaction. Table II lists the intensity of muons and taus above 10 PeV of the energy loss for the fluxes of the cosmogenic [22] and top-down [6] models. The event rate under this criterion is found to be $0.27(\mu+\tau)/\mathrm{km}^2\,\mathrm{yr}$ for cosmogenic neutrino fluxes with moderate source evolution. Note that the downward event rate is $0.25/\mathrm{km}^2$ yr and dominates in the overall rate. The event rates for the various neutrino production models are summarized in Table III.

The IceCube sensitivity to EHE neutrinos can be evaluated by the event rate per energy decade $dN/d\log E$. For a given energy of primary neutrinos, the secondary muon and tau fluxes are calculated by the transport equations Eqs. (3) and (4) as a function of zenith angles. The probability that

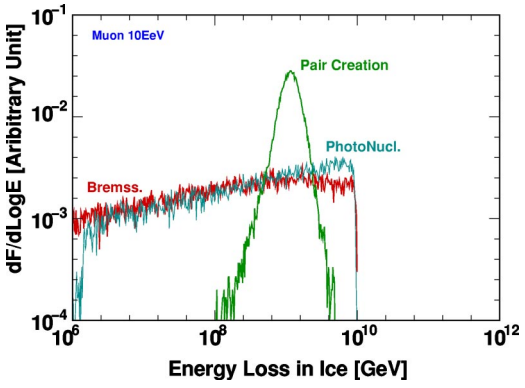

FIG. 7. Distribution of energy loss in propagation of muons over 1 km in ice. The primary energy of muons is 10^{10} GeV. Contributions from each interaction are shown separately.

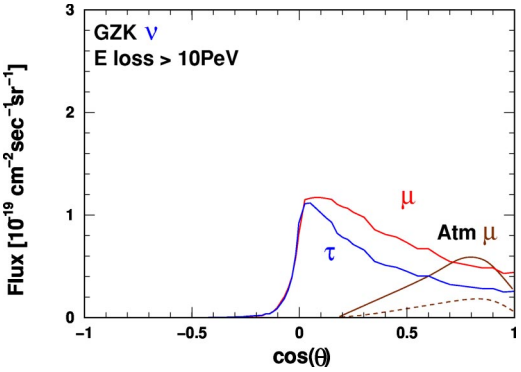

FIG. 8. Dependence of the muon and tau fluxes originating in the cosmogenic neutrinos on the cosine of zenith angle. The integral flux above 10 PeV of the energy loss is plotted on a linear scale. The atmospheric muon fluxes are also shown by the solid curve for the conservative estimation with the low energy extrapolation and by the dashed curve for the CORSIKA-based estimation.

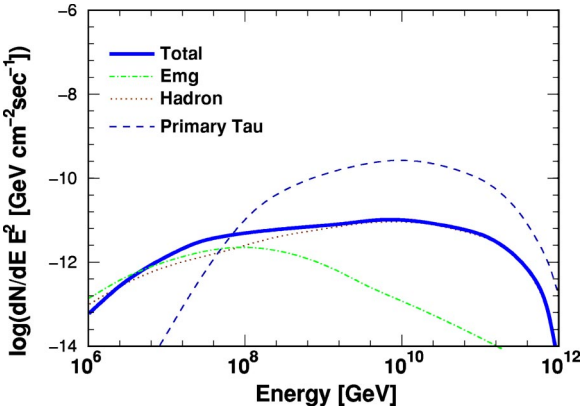

FIG. 9. The tau fluxes at IceCube depth originating in the cosmogenic neutrinos as a function of energy (the dashed curve), total energy loss in ice (the solid curve), energy loss in the form of electromagnetic cascades (the dash-dotted curve), and in the form of hadronic cascades (the dotted curve).

energy loss with the threshold value or greater occurs is estimated by a Monte Carlo simulation and convoluted with flux integration over energy and zenith angle to give the rate. Figure 10 shows the resulting sensitivity of the IceCube detector with 1 km^2 detection area. The various model predictions are also shown for comparison. The 90% C.L. upper limit, i.e., 2.3 event/energy decade/10 yr is plotted for a 10 PeV and 1 PeV threshold of the energy loss, respectively. The ν_μ sensitivity is better than that for ν_τ below the 10^8 GeV region because muon energy loss in a detection volume is larger than that of taus with the same energy, but tau decay, which results in a large energy deposit in the detection volume, makes the dominant contribution in ν_τ sensitivity in this relatively low energy range, forming a slight bump structure in the sensitivity curve. The 90% C.L. upper limit of EHE neutrino fluxes in a km^2 detection area would be placed at $E^2dF/dE \simeq 3.7\times10^{-8}$ GeV/cm^2 sec sr for ν_μ and 4.6×10^{-8} for ν_τ with energies of 10^9 GeV in the absence of signals with energy loss in a detection volume of 10 PeV or greater.

This bound would not exclude the cosmogenic neutrino production model but strongly constrains the cosmic ray injection spectrum in the model. Cosmic ray nucleon injection spectra harder than $E^{-1.5}$ would violate the bound [25]. On the other hand, as long as the injection spectrum is softer than E^{-2}, which is very likely in the case of astrophysical cosmic ray sources, the IceCube bound would constrain the source evolution less as seen in Fig. 10, where we plotted an extreme scenario of cosmological evolution $(1+z)^5$ where z is the redshift [25]. Stronger evolution possibilities than this case are inconsistent with the diffuse background γ-ray observation by EGRET [30], since the GZK mechanism also initiated electromagnetic cascades [22,23,25] via photoproduced π^0 decay and $e^\pm$ pair creation by EHECR collisions with CMB photons, forming the photon flux below 100 GeV which is constrained by the observation.

The topological defect scenario, on the other hand, would be severely constrained by the absence of EHE event detection by IceCube. The expected event rate is $\sim$2 events/yr km^2 as one can calculate from Table II. The expected EHE neutrino flux in the Z burst model [31], the scenario that the collisions of EHE neutrinos with the cosmological background neutrinos explain the EHECR fluxes without the GZK cutoff, is well below the IceCube bound if the injection neutrino spectrum is E^{-1} as described in Ref. [32].

Although less significant, there are μ and τ events produced by neutrinos *inside* the detector instrumented volume. In this case the charged leptons produced propagate in only a part of the observation volume. We carried out the same Monte Carlo simulation deriving the results of Fig. 7 but in which ν_μ and ν_τ were initially entering into the ice volume. The probability that neutrinos interact inside the 1 km^3 volume and that the produced muon or tau loses energy greater than 10 PeV was estimated and convoluted with the neutrino intensity at the IceCube depth. The detection sensitivities by this channel are shown as thick dashed curves in Fig. 10. In the EHE regime above $\sim10^8$ GeV, the intensity of internally produced muon and tau events is too small to contribute to the overall sensitivity because the neutrino target volume is limited by the size of the detector, i.e., 1 km^3. Below 10^8 GeV, on the other hand, including this channel improves the sensitivity in a sizable manner because the energy losses of muons and taus during their propagation over long distances are more likely to transfer them out of the energy range above the 10 PeV threshold, which leads to reduction of the effective neutrino target volume for producing EHE

TABLE III. The event rates for several EHE neutrino models. The notation for the model name is the same as in Table II.

	$N_\mu(E_{loss}\geqslant 10$ PeV) (km^{-2} yr^{-1})	$N_\tau(E_{loss}\geqslant 10$ PeV) (km^{-2} yr^{-1})
GZK downward	0.15	0.10
GZK upward	0.0081	0.0083
TD downward	1.18	0.93
Atmospheric μ	0.055	—
Atmospheric μ (CORSIKA)	0.016	—

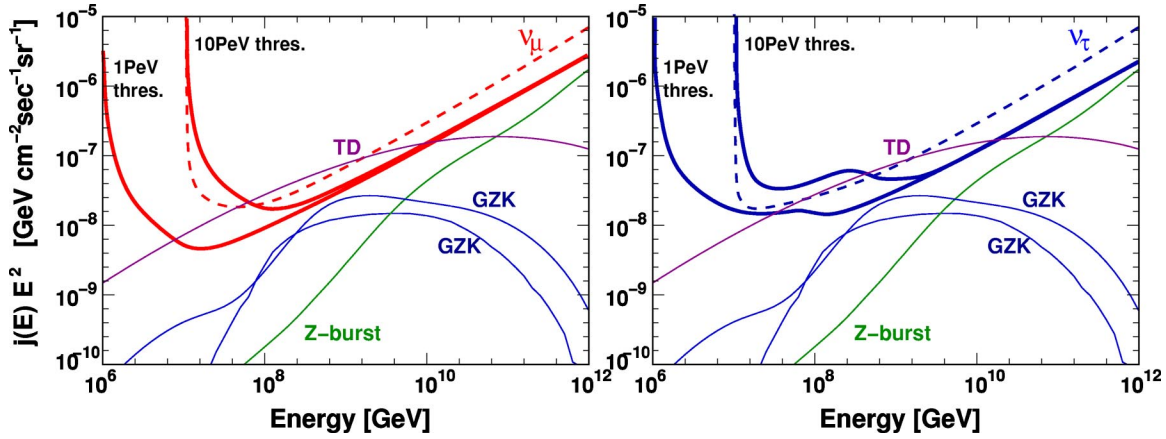

FIG. 10. The IceCube sensitivities to the EHE neutrino fluxes. 90% C.L. limits with a 1 km^2 detection area with 10 yr observation are drawn. The left panel shows the case of ν_μ and the right panel shows the ν_τ case. Labels refer to GZK ([22] for the lower curve, [25] for the upper curve), TD [6], and *Z* burst [32]. The dashed curves show the sensitivities determined by events of neutrinos interacting inside the detector volume.

muons and taus outside the detector volume. There is little gain in EHE neutrino searches, however, because the proposed EHE neutrino models have their main energy range above 10^8 GeV.

V. SUMMARY AND OUTLOOK

We calculated the propagation of the EHE neutrinos and charged leptons in Earth to derive their intensities and their dependence on nadir angle. The secondarily produced muons and taus form detectable fluxes at the IceCube depth, with an intensity three orders of magnitude lower than the neutrino fluxes. A realistic criterion, requiring energy deposit greater than 10 PeV in 1 km^3 volume of ice, leads to $\sim$0.27 events/yr for the cosmogenic neutrinos in the case of moderate source evolution. The topological defect scenario would be severely constrained.

The atmospheric muon background is likely to be negligible even for downgoing events. The background rate is $\sim$0.05 event/km^2 yr. It should be noted that we ignored the possible contributions of prompt muons from the charm decay in EHE cosmic ray air showers [33], however. The atmospheric muon intensity can be increased by an order of magnitude but a large uncertainty remains due to highly uncertain cross sections in charm production. The mass composition of cosmic rays in the relevant energy range would also be a deciding factor of the prompt muon flux intensity: It can be reduced by an order of magnitude if the cosmic rays are heavy nuclei [34] and may not constitute a background in the EHE neutrino search. Even if the prompt muon intensity is sizable, their energy spectrum will still be much steeper than the expected spectrum in the proposed EHE cosmic neutrino models, however, and one can easily distinguish the signal detections from the prompt muon background events if the neutrino observatory has reasonable resolution for the energy loss of muon and tau tracks. The detector resolution issues require detailed detector Monte Carlo simulations for further investigations. The AMANDA experience in relatively low energy muon reconstruction would lead to energy resolution of $\Delta \log E \simeq 0.3$ [35]. The development of a detector Monte Carlo simulation is in progress and its application to the present results will be important future work toward the search for EHE neutrinos by the IceCube observatory.

ACKNOWLEDGMENTS

We wish to acknowledge the IceCube Collaboration for useful discussions and suggestions. We thank Dmitry Chirkin, Thomas Gaisser, and Esteban Roulet for helpful discussions on atmospheric muon issues. We also thank John Beacom and Igor Sokalski for their valuable comments. Special thanks go to Mary Hall Reno for providing the cross section table evaluated by the CTEQ version 5 parton distribution. This work was supported in part by Grants-in-Aid (Grants No. 15403004 and No. 15740135) in Scientific Research from the MEXT (Ministry of Education, Culture, Sports, Science, and Technology) in Japan.

[1] For a review see, e.g., M. Nagano and A.A. Watson, Rev. Mod. Phys. **72**, 689 (2000); J.W. Cronin, *ibid.* **71**, S165 (1999); S. Yoshida and H. Dai, J. Phys. G **24**, 905 (1998).
[2] V.S. Beresinsky and G.T. Zatsepin, Phys. Lett. **28B**, 423 (1969).
[3] K. Greisen, Phys. Rev. Lett. **16**, 748 (1966); G.T. Zatsepin and V.A. Kuzmin, Pis'ma Zh. Eksp. Teor. Fiz. **4**, 114 (1966) [JETP Lett. **4**, 78 (1966)].
[4] P. Bhattacharjee, C.T. Hill, and D.N. Schramm, Phys. Rev. Lett. **69**, 567 (1992).
[5] G. Sigl, S. Lee, D.N. Schramm, and P.S. Coppi, Phys. Lett. B **392**, 129 (1997).
[6] G. Sigl, S. Lee, P. Bhattacharjee, and S. Yoshida, Phys. Rev. D **59**, 043504 (1999).
[7] J. Alvarez-Muñiz and F. Halzen, Phys. Rev. D **63**, 037302 (2001).

[8] J. Jones, I. Mocioiu, M.H. Reno, and I. Sarceiv, Phys. Rev. D (to be published), hep-ph/0308042.
[9] J.L. Feng, P. Fisher, F. Wilczek, and T.M. Yu, Phys. Rev. Lett. **88**, 161102 (2003); K. Giesel, J.-H. Jureit, and E. Reya, Astropart. Phys. **20**, 335 (2003).
[10] J.F. Beacom, P. Crotty, and E.W. Kolb, Phys. Rev. D **66**, 021302 (2002).
[11] S. Yoshida, in Proceedings of the 28th ICRC, H.E.2.3, 1369, 2003; http://icecube.wisc.edu/
[12] S. Kelner, R.P. Kokoulin, and A.A. Petrukhin, Phys. At. Nucl. **63**, 1603 (2000).
[13] R.P. Kokoulin and A.A. Petrukhin, in Proceedings of the 12th ICRC (Hobert), Vol. 6, p. A2436, 1971; S.R. Kelner, R.P. Kokoulin, and A.A. Petrukhin, Phys. At. Nucl. **62**, 1894 (1999).
[14] Yu.M. Andreev, L.B. Bezrukov, and E.V. Bugaev, Phys. At. Nucl. **57**, 2066 (1994); S.R. Kelner, R.P. Kokoulin, and A.A. Petrukhin, *ibid.* **60**, 576 (1997); I.A. Sokalski, E.V. Bugaev, and S.I. Klimushin, Phys. Rev. D **64**, 074015 (2001).
[15] S. IyerDutta, M.H. Reno, I. Sarcevic, and D. Seckel, Phys. Rev. D **63**, 094020 (2001).
[16] H. Abramowicz and A. Levy, hep-ph/9712415.
[17] R. Gandhi, C. Quigg, M.H. Reno, and I. Sarcevic, Astropart. Phys. **5**, 81 (1996); Phys. Rev. D **58**, 093009 (1998).
[18] CTEQ Collaboration, H. Lai *et al.*, Phys. Rev. D **55**, 1280 (1997).
[19] T.K. Gaisser, *Cosmic Rays and Particle Physics* (Cambridge University Press, Cambridge, England, 1990).
[20] S.I. Dutta, M.H. Reno, and I. Sarcevic, Phys. Rev. D **62**, 123001 (2000).
[21] A.M. Dziewonsky and D.L. Anderson, Phys. Earth Planet. Inter. **25**, 297 (1981); S.V. Panasyuk, http://cfauvcs5.harvard.edu/lana/rem/index.html
[22] S. Yoshida and M. Teshima, Prog. Theor. Phys. **89**, 833 (1993).
[23] R.J. Protheroe and P.A. Johnson, Astropart. Phys. **4**, 253 (1996).
[24] R. Engel, D. Seckel, and T. Stanev, Phys. Rev. D **64**, 093010 (2001).
[25] O.E. Kalashev, V.A. Kuzmin, D.V. Semikoz, and G. Sigl, Phys. Rev. D **66**, 063004 (2002).
[26] SuperKamiokande Collaboration, Y. Fukuda *et al.*, Phys. Rev. Lett. **85**, 3999 (2000).
[27] I. Sokalski (private communication).
[28] V. Agrawal, T.K. Gaisser, P. Lipari, and T. Stanev, Phys. Rev. D **53**, 1314 (1996).
[29] D. Heck *et al.*, Report No. FZKA **6019**, Forschungszentrum Karlsruhe, 1998.
[30] P. Sreekumar *et al.*, Astrophys. J. **494**, 523 (1998).
[31] D. Fargion, B. Mele, and A. Salis, Astrophys. Lett. **517**, 725 (1999); T.J. Weiler, Astropart. Phys. **11**, 303 (1999).
[32] S. Yoshida, G. Sigl, and S. Lee, Phys. Rev. Lett. **81**, 5505 (1998).
[33] See, e.g., T.S. Sinegovskaya and S.I. Sinegovsky, Phys. Rev. D **63**, 096004 (2001), and references therein.
[34] J. Candia and E. Roulet, J. Cosmol. Astropart. Phys. **09**, 005 (2003).
[35] IceCube Collaboration, J. Ahrens *et al.*, astro-ph/0305196.